

# A LATTICE MODEL FOR LIQUID TRANSPORT IN CRACKED UNSATURATED HETEROGENEOUS POROUS MATERIALS

Peter Grassl\*, Caroline Fahy\*, Domenico Gallipoli<sup>†</sup> and John Bolander<sup>‡</sup>

\*University of Glasgow  
School of Engineering, Glasgow, UK,  
Rankine Building, University of Glasgow, G12 8QQ,  
emails: peter.grassl@glasgow.ac.uk, c.fahy.1@research.gla.ac.uk

<sup>†</sup>Université de Pau et des Pays de l'Adour, France  
Laboratoire SIAME, France  
email: domenico.gallipoli@univ-pau.fr

<sup>‡</sup>University of California, Davis  
One Shields Avenue, Davis, CA 95616, USA  
email: jebolander@ucdavis.edu

**Key words:** Concrete, Fracture mechanics, Unsaturated flow, Meso-scale, Lattice, Coupling

**Abstract.** Fracture increases the permeability of cementitious materials, which is known to accelerate their deterioration when exposed to aggressive environments. The coupling of fracture and flow is therefore important for modelling the durability of these materials. Lattice models are suitable for this in that they describe well the discontinuities that arise from fracture processes and are capable of modelling flow accurately. This paper describes progress made in developing an approach to couple irregular lattices of beam-like elements representing mechanical behaviour (i.e. elasticity and fracture) and conduit elements representing mass transport. The transport part of the model is used to describe absorption of water in concrete using principles developed originally for unsaturated soils. The effect of fracture on transport is considered by adjusting the transport properties of the conduit elements according to a cubic function of the crack opening. The modelling is applied to several benchmarks and extended to consider the meso-structure of concrete in the form of randomly arranged circular inclusions. The influence of inclusion volume fraction on the change of water content is studied.

## 1 Introduction

Concrete is one of the most common building materials to suffer from water ingress. Given that concrete is widely used in all aspects of construction, transport models are often needed for predicting the extent of moisture movement and, hence, to gauge the condition of structures. Furthermore, it is known that fracture facilitates the water ingress. In this context, a mass transport model is proposed to describe

the movement of liquid through partly saturated porous fractured concrete. The proposed model is based on a lattice approach that uses a randomly generated dual Delaunay and Voronoi tessellation of the material domain [1, 2]. The constitutive retention and permeability laws of the porous material are based on the hydraulic functions originally proposed by [3] and [4] for unsaturated soils and subsequently modified by [5]. The effect of fracture on transport is con-

sidered by adjusting the transport properties of the conduit elements according to a cubic function of the crack opening [6]. The lattice model incorporating the above constitutive laws is applied to two benchmark problems (in 1D and 2D, respectively) to demonstrate its numerical robustness and ability to describe liquid movement through porous media.

## 2 Lattice model

The present two-dimensional numerical model for the coupling of the movement of liquid under the gradient of hydraulic potential and fracture is based on lattices of one-dimensional structural and conduit elements. The spatial arrangement of the lattice elements and their cross-sectional properties are based on Delaunay and Voronoi tessellations of the domain shown in Figure 1.

For the mechanical lattice, the elements are placed on the edges of the Delaunay triangles. The geometry of the mid cross-section of the lattice elements is determined by the corresponding edge of the Voronoi polygon of length  $l$ . Each node has three degrees of freedom, that is two translations  $u$  and  $v$  and one rotation  $\phi$ , which determine the displacement jump at the centroid  $C$  of the element's mid cross-section (Figure 2). The displacement jumps are transformed into strains by the element length  $h$ . An isotropic damage model is used to relate the strains to stresses. The evolution of damage is controlled by a stress-crack opening curve, so that the mechanical response is independent of the length of the lattice elements used. A more detailed description of the mechanical lattice and constitutive model can be found in [1] and [2], respectively. Transport elements are placed along the facets of the Voronoi polygons and their cross-sectional areas are calculated from the length of the corresponding edges of the dual Delaunay triangles. The material response of the transport elements is calculated, as for the structural elements, at point  $C$  (Figure 2). This simplifies the transfer of information from the structural to transport lattice and vice versa.

For the application of the lattice model in this work, both homogeneous and heterogeneous material properties are considered. The heterogeneity of the material is represented by randomly arranged circular inclusions with varying diameter which are projected onto the lattice. Depending on the position of lattice elements relative to the inclusions, the properties of the elements represent either those of the matrix or the inclusions. For the interface between matrix and inclusions, the lattice nodes are placed at special locations, such that the mid cross-sections of the mechanical lattice elements form the boundaries between inclusions and matrix [7]. The arrangement of the mechanical lattice elements with respect to the inclusions is shown in Figure 3a. In the present work, inclusions are assumed to be impermeable and are, therefore, not discretised by transport elements (Figure 3b).

Transport elements are idealised as one-dimensional conductive pipes [7]. The gradient of hydraulic head, which governs flow rate along each transport element, is determined from the capillary pressures  $P_c$  at the two nodes. Figure 2 shows one transport element together with the capillary pressures acting at the nodes and the associated cross-sectional area as obtained from the dual Delaunay triangle. In this work we restrict our attention to the case where pore water is in tension and, in the following, liquid pressure is therefore referred to as capillary pressure. The mass balance equation describes the change in moisture inside a porous element as a consequence of liquid flow and solid-liquid retention. A positive sign is assumed for liquid tension, unlike the convention of soil mechanics which assumes compression positive. For the balance equation, the following differential expression is obtained:

$$c \frac{\partial P_c}{\partial t} - k \operatorname{div} \left( \nabla \left( \frac{P_c}{g} - \rho z \right) \right) = 0 \quad (1)$$

where  $c$  is the mass capacity,  $k$  is the hydraulic conductivity,  $g$  is the acceleration of gravity,  $z$  is the capillary height and  $t$  is the time. Boundary conditions are imposed either as prescribed

values of capillary pressure (on boundary  $\Gamma_1$ ) or as prescribed values of flux (on boundary  $\Gamma_2$ ). The latter boundary condition can then be related to the gradient of capillary pressure through Darcy's law. This results in the following two mathematical constraints on  $P_c$ :

$$P_c = g(\mathbf{x}) \text{ on } \Gamma_1 \text{ and } \frac{\partial P_c}{\partial \mathbf{n}} = \mathbf{f}(\mathbf{x}) \text{ on } \Gamma_2 \quad (2)$$

where  $\mathbf{n}$  denotes the direction normal to the boundary while  $g(\mathbf{x})$  and  $\mathbf{f}(\mathbf{x})$  are functions of the spatial coordinate vector  $\mathbf{x}$ .

The discrete form of the differential equation for mass transport in (1) for a one-dimensional transport element is

$$\boldsymbol{\alpha}_e \mathbf{P}_c + \mathbf{C}_e \frac{\partial \mathbf{P}_c}{\partial t} = \mathbf{f}_e \quad (3)$$

where  $\mathbf{P}_c$  is a vector containing the nodal values of the capillary pressure,  $\boldsymbol{\alpha}_e$  is the conductivity matrix,  $\mathbf{C}_e$  is the capacity matrix and  $\mathbf{f}_e$  is the nodal flow rate vector. The influence of the capillary height  $z$  in (1) is modelled by a flow vector analogous to the way of considering body forces in structural problems.

The capacity matrix is

$$\mathbf{C}_e = \frac{A\ell}{12} c \begin{pmatrix} 2 & 1 \\ 1 & 2 \end{pmatrix} \quad (4)$$

where  $c$  is the capacity of the material. Furthermore, the conductivity matrix is defined as

$$\boldsymbol{\alpha}_e = \frac{A}{\ell} k \begin{pmatrix} 1 & -1 \\ -1 & 1 \end{pmatrix} \quad (5)$$

where  $k$  is the hydraulic conductivity and  $A = hb$  is the cross-sectional area. Here,  $b$  is the out-of-plane thickness of the element assuming a rectangular cross-section.

### 3 Constitutive laws

The mass transport equation in (1) and its discrete form in (3) are based on the constitutive laws for the capacity  $c$  and the hydraulic conductivity  $k$ . The capacity  $c$  is defined as

$$c = -\rho \frac{\partial \theta}{\partial P_c} \quad (6)$$

where  $\theta$  is the volumetric water content which is calculated by a modified version of van Genuchten's retention model proposed in [5]. The presence of a crack in an element does not influence the capacity in the present model. The volumetric water content is

$$\theta = S_e (\theta_s - \theta_r) + \theta_r \quad (7)$$

where  $\theta_r$  and  $\theta_s$  are the residual and saturated water contents corresponding to effective saturation values of  $S_e = 0$  and  $S_e = 1$ , respectively. The effective degree of saturation  $S_e$  is defined as

$$S_e = \begin{cases} \Xi \left( 1 + \left( \frac{P_c}{a} \right)^{\frac{1}{1-m}} \right)^{-m} & \text{if } P_c \geq P_{c(\text{aev})} \\ 1 & \text{if } P_c < P_{c(\text{aev})} \end{cases} \quad (8)$$

in which  $a$ ,  $m$  are model parameters. In (8),

$$\Xi = \frac{\theta_m - \theta_r}{\theta_s - \theta_r} \quad (9)$$

where  $\theta_m$  is an additional model parameter and  $P_{c(\text{aev})}$  is the air-entry value of capillary pressure which separates saturated ( $P_c < P_{c(\text{aev})}$ ) from unsaturated states ( $P_c > P_{c(\text{aev})}$ ). From the physical point of view, air breaks into an initially saturated material when capillary tension exceeds  $P_{c(\text{aev})}$  (hence inducing a drop of degree of saturation). Conversely, water floods all pores of an initially unsaturated material when capillary tension falls below  $P_{c(\text{aev})}$  (hence attaining a degree of saturation of one). It is intuitive that the smaller the pore size of the material, the larger the value of  $P_{c(\text{aev})}$  will be. The role of parameter  $\Xi$  is illustrated in Figure 4 which provides a schematic representation of the saturation-pressure law in (8).

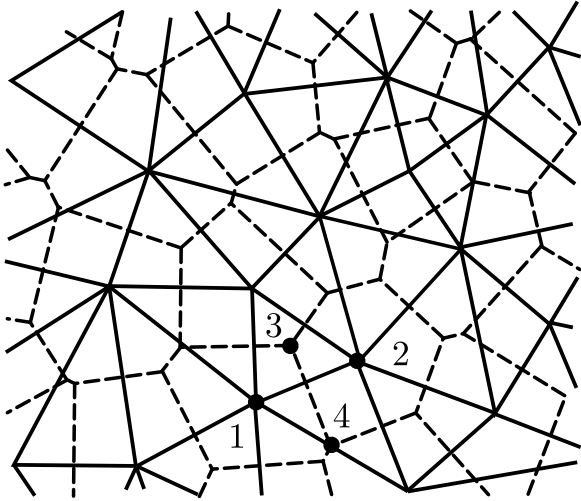


Figure 1: Dual lattice model for fracture and transport: Delaunay triangulation (solid lines) and Voronoi tessellation (dashed lines).

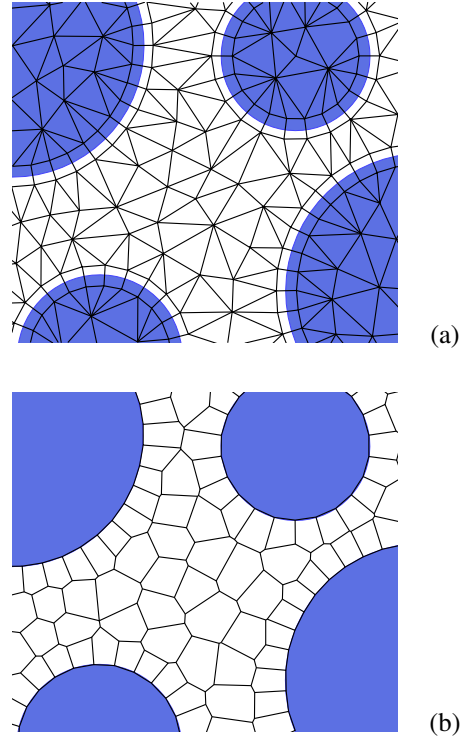


Figure 3: Lattice element arrangement around inclusions: (a) Mechanical elements and (b) transport elements.

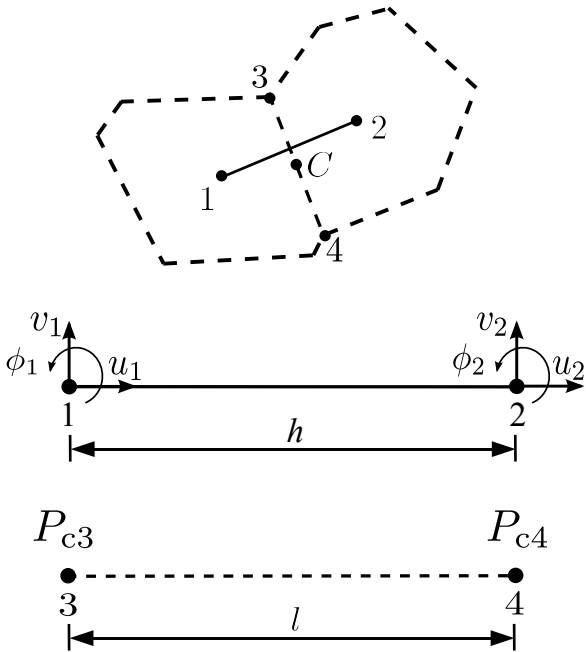


Figure 2: Dual lattice model for fracture and transport: Mechanical and transport elements.

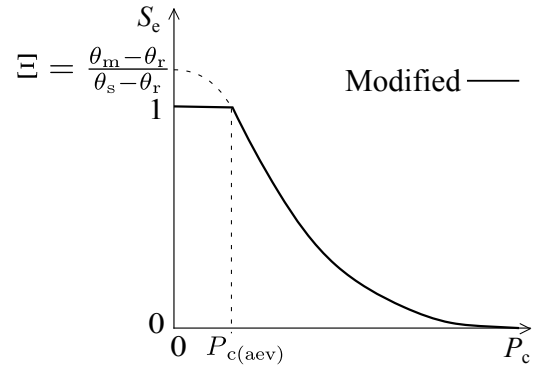


Figure 4: Effective degree of saturation  $S_e$  versus capillary pressure  $P_c$  for the modified van Genuchten model.

By setting  $S_e = 1$  in (8), the air-entry value of capillary pressure  $P_c = P_{c(aev)}$  is calculated as

$$P_{c(aev)} = a (\Xi^{1/m} - 1)^{1-m} \quad (10)$$

The hydraulic conductivity  $k$  in (5) consists of

$$k = k_0 + k_c \quad (11)$$

where  $k_0$  is the hydraulic conductivity of the intact material and  $k_c$  is the additional conductivity due to cracking. The part  $k_0$  is expressed in terms of intrinsic conductivity  $\kappa$ , relative conductivity  $\kappa_r$ , density of water  $\rho$  and absolute (dynamic) viscosity of water  $\mu$  as

$$k_0 = \frac{\rho g}{\mu} \kappa \kappa_r \quad (12)$$

The relative conductivity  $\kappa_r$  is a function of the effective degree of saturation and is defined as

$$\kappa_r = \sqrt{S_e} \left( \frac{1 - \left[ 1 - \left( \frac{S_e}{\Xi} \right)^{1/m} \right]^m}{1 - \left[ 1 - \left( \frac{1}{\Xi} \right)^{1/m} \right]^m} \right)^2 \quad (13)$$

If  $\theta_m = \theta_s$ , equation (9) reduces to  $\Xi = 1$  and (13) reduces to the expression of the relative conductivity of the original van Genuchten model. The cracking part is

$$k_c = \xi \frac{\rho g}{\mu} \frac{\tilde{w}_c^3}{12h} \quad (14)$$

where  $\xi$  is a tortuosity factor taking into account the roughness of the crack surface,  $\tilde{w}_c$  is the equivalent crack opening of the mechanical lattice and  $h$  is the length of the mechanical element.

## 4 Analyses

### 4.1 1D analysis

To verify that the transport constitutive equations of Section 3 are correctly implemented, the 1D capillary infiltration problem investigated by [5] was modelled again in the present study. Table 1 gives the parameter values of the modified van Genuchten model [5] as used in the simulations while Figure 5 shows the corresponding variations of volumetric water content  $\theta$ , water capacity  $c$  and relative conductivity  $\kappa_r$  with capillary pressure  $P_c$ .

Prior to the start of the analysis, the 1 m soil column in Figure 6a is assumed to be in hydraulic equilibrium with an imposed capillary

pressure of 0.0981 MPa at the bottom (see Figure 6b). This value of capillary pressure corresponds to an imposed pressure head of  $-10$  m as specified in [5]. At time zero, atmospheric pressure was imposed at the bottom of the column combined with a zero flux at the top (Figure 6c), leading to an upward infiltration (i.e. an infiltration against gravity). As can be seen in Figure 7, the wetting fronts predicted by the lattice approach agree well with those presented in [5].

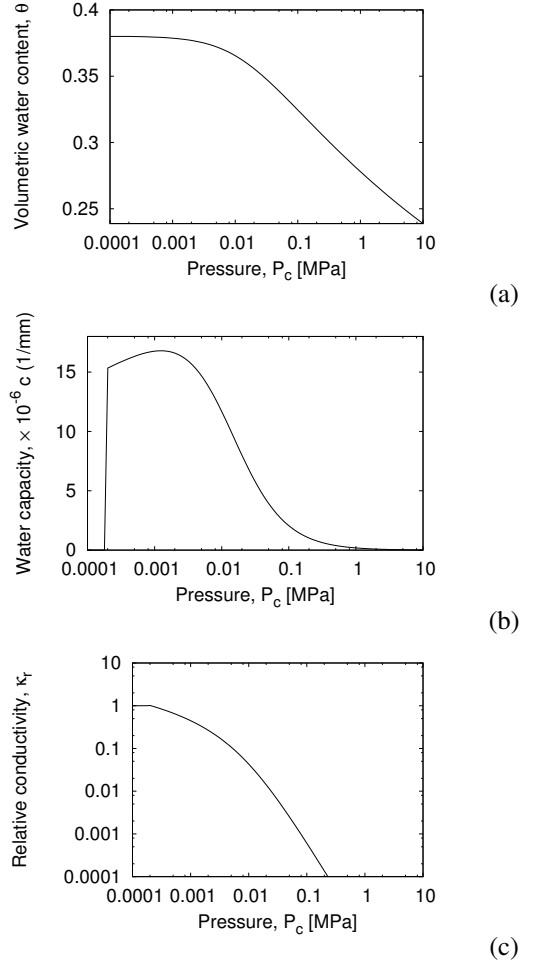


Figure 5: Constitutive responses used in the 1D analysis: (a) Volumetric water content versus capillary pressure and (b) water capacity versus capillary pressure and (c) relative conductivity versus capillary pressure.

**Table 1:** Parameters for 1D soil column analysis.

$\theta_s$	0.380
$\theta_r$	0.068
$\theta_m$	0.3803
$\mu$ [t/(mms)]	$1 \times 10^{-9}$
$\kappa$ [mm <sup>2</sup> ]	$5.6634 \times 10^{-8}$
$m$	0.0826
$a$ [MPa]	0.0123

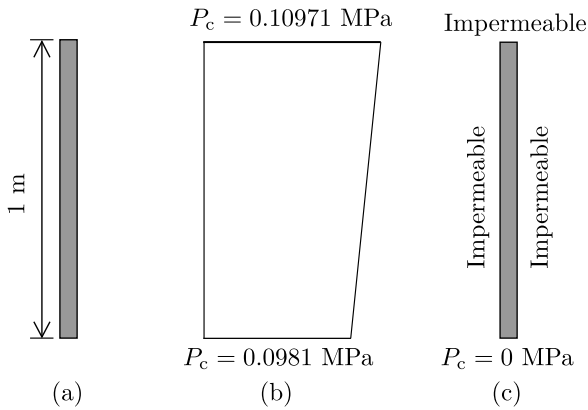
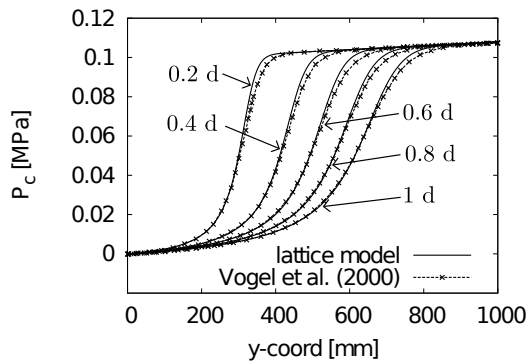

 Figure 6: (a) Geometry, (b) Initial pressure distribution, i.e. prior to start ( $t < 0$ ) and (c) Boundary conditions at start of the analysis ( $t = 0$ ).


Figure 7: Comparison of capillary pressure versus specimen height at different times obtained by the lattice model and against results reported by Vogel et al. [5] using the modified van Genuchten model.

## 4.2 2D analysis

The dual lattice modelling approach presented in the previous section is applied to

model water absorption in cracked and uncracked concrete and compared to experimental results reported by Wittmann and co-workers in [8]. This experimental study consists of two parts in which the bottom surfaces of uncracked and cracked concrete beams are subjected to contact with water. The absorption of water into the unsaturated concrete was measured in the experiments by means of neutron radiography. The idealised geometry for the present 2D modelling of the experiments is shown in Figure 8. For the cracked concrete beam, an equivalent crack opening of  $\tilde{w}_c = 0.35$  mm at the bottom of the beam was used in accordance with the experimental study. The model parameters used for the transport analyses are shown in Table 2. Here, the parameters  $a$  and  $m$  were taken from [9]. Since  $\theta_s = \theta_m$  in Table 2, the expressions of capacity and relative conductivity in (6) and (13), respectively, reduce to those of the original van Genuchten model.

**Table 2:** Parameters for 2D concrete beam analysis.

$\theta_s$	0.0924
$\theta_r$	0
$\theta_m$	0.0924
$\mu$ [t/(mms)]	$1 \times 10^{-9}$
$\kappa$ [mm <sup>2</sup> ]	$1 \times 10^{-13}$
$m$	0.4396
$a$ [MPa]	18.6237
$\rho$ [t/(mm <sup>3</sup> )]	$1 \times 10^{-9}$

In the numerical analyses, the beams were assumed to be partially saturated with an initial effective saturation of  $S_e = 0.5$  and the results are presented in the form of a change of water content. The parameter  $\theta_s = 0.0924$  in Table 2 was chosen assuming a maximum change of water content of  $\Delta\theta = 0.0462$  (taken from [8]) and an initial saturation of  $S = 0.5$ . The value for water density and dynamic viscosity are obtained from standard tables. The tortuosity parameter  $\xi$  was taken from [10]. Only the intrinsic permeability was adjusted to match the water content distribution curves reported in the experiments at a time of 15 min. The chosen in-

trinsic permeability lies within the range of values observed in experiments.

For the uncracked case the results are presented in Figure 9 in the form of a contour plot of the capillary pressure  $P_c$ . Only the centre of the beam is shown. The water content distribution obtained in the analysis for a vertical section in the middle of the uncracked beam (dashed line in Figure 8b) is compared to experimental results in Figure 10 for water absorption up to 8 h. For the first 4 time steps, the water content curves are represented well by the model, which is expected as the intrinsic conductivity was chosen to fit the water content profile for a time of 15 min. However, for greater times the lattice model overestimates the water absorption.

The second part of the analyses involved the modelling of water absorption for a cracked concrete beam. Firstly, the mechanical lattice was used to simulate the three point bending test shown in Figure 8a. This loading setup results in one main crack propagating from the bottom in the middle of the beam to the top. At a maximum equivalent crack opening of  $\tilde{w}_c = 0.35$  mm, the mass transport analysis was performed. The resulting contour plots of the capillary pressure  $P_c$  for the water transport analysis of the cracked beam are shown in Figure 11. Only the centre of the beam is shown. It can be seen that water is transported through the crack into the concrete beam. In addition, transport from the crack into the surrounding concrete is visible. The model and experimental results are compared in the form of change of water content versus the  $x$ -coord along the length of the beam at mid-height (Figure 12). The change of water content within the crack ( $x = 0$ ) is overestimated by the model. However, the penetration depth into the surrounding concrete is captured well by the numerical approach.

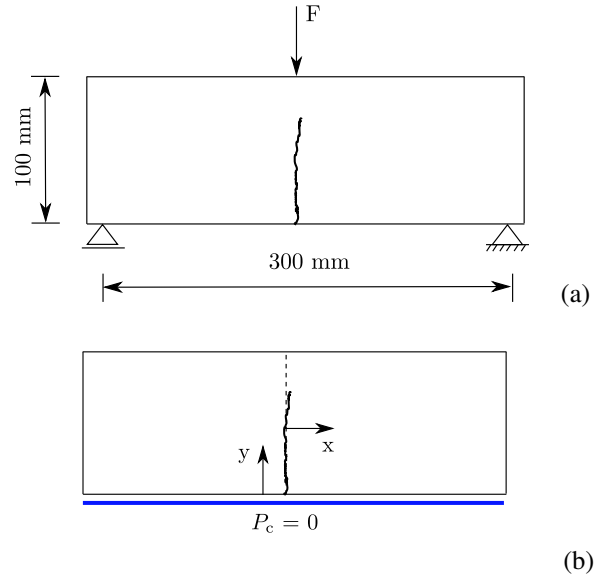


Figure 8: Geometry and loading setup for the three-point bending beam: (a) mechanical loading to induce cracking, (b) transport.

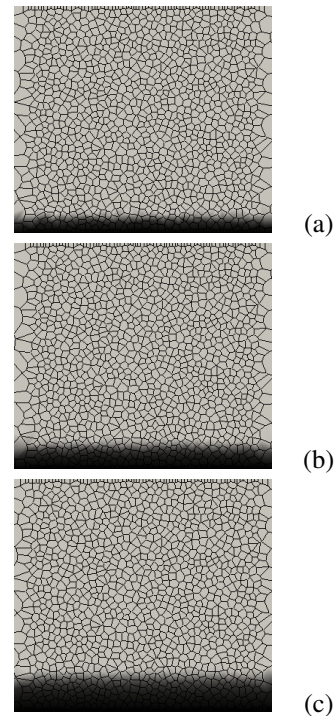


Figure 9: Contour plots of the distribution of capillary pressure for three time steps for the uncracked beam. Black corresponds to  $P_c = 0$  MPa ( $S = 1$ ) and the lightest gray shade corresponds to  $P_c = 39.58$  MPa ( $S = 0.5$ ).

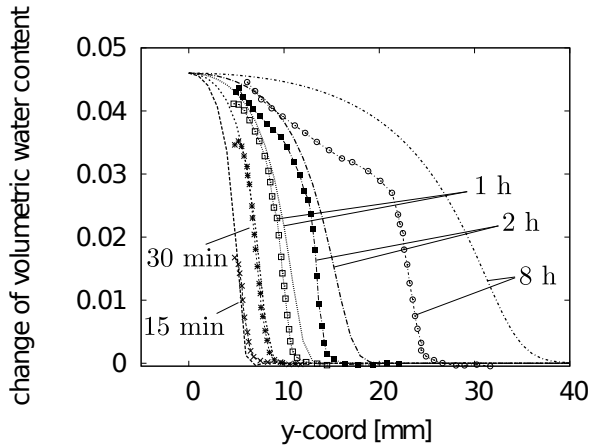


Figure 10: Change of water content versus y-coord along the ligament of the uncracked beam: Lattice results (lines) against experimental results (lines with symbols) reported in [8].

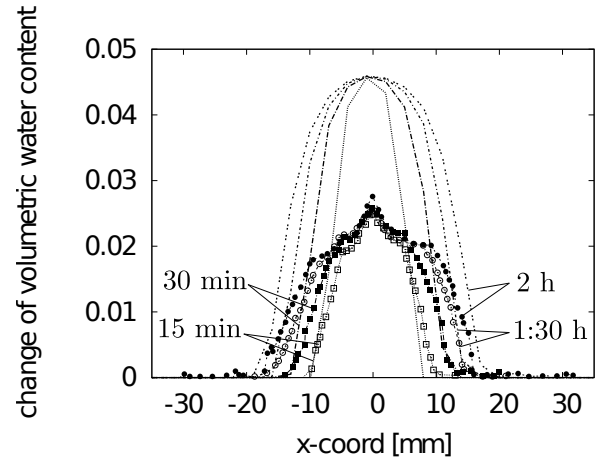


Figure 12: Change of water content versus x-coord along the mid-height of the cracked beam: Lattice results (lines) against experimental results (lines with symbols) reported in [8].

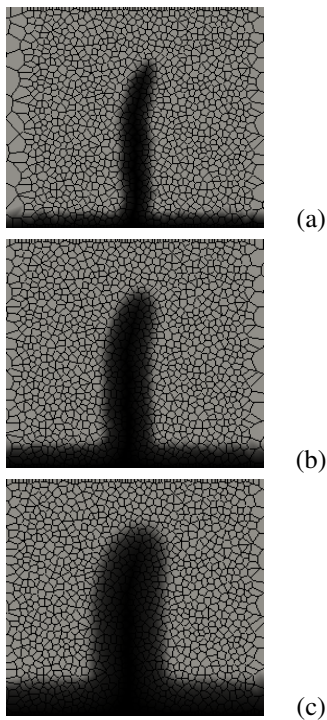


Figure 11: Contour plots of the distribution of capillary pressure for three time steps for the cracked beam. Black corresponds to  $P_c = 0$  MPa ( $S = 1$ ) and the lightest gray shade corresponds to  $P_c = 39.58$  MPa ( $S = 0.5$ ).

### 4.3 2D meso-scale analysis

In section 4.2, concrete was modelled as a homogeneous material. Using this assumption, the lattice results agree well with the experimental data for the first hour of the absorption process. However, for later stages, the model predictions overestimate the water absorption observed in experiments. In the recent work by Wang and Ueda in [11], the heterogeneity of the material in the form of impermeable inclusions has been considered for the modelling of the absorption of water by a meso-scale analysis. In their study, the total amount of absorbed water has been shown to be in good agreement with experimental results even for later stages for which in the present homogeneous analyses the water absorption was overestimated (Figure 10). However, no information on the influence of inclusions on the water content change profiles was presented in Wang and Ueda's work [11].

In the present study, the influence of heterogeneity on the water change profiles is investigated in more detail. Three inclusion volume fractions  $\rho_a = 0.2, 0.3$  and  $0.4$  are modelled to investigate the influence of inclusions on the absorption process. The lattices in Figure 13 are finer than for the homogeneous analysis in the previous section so that the closely

spaced circular inclusions for the volume fraction  $\rho = 0.4$  can be discretised. The inclusions are considered to be impermeable and are, therefore, not discretised by transport elements (see Figure 13). The profiles of change of water content is evaluated by subdividing the mid region of the beam (over a width of 0.1 m) by a regular grid of cells. The water content in the x-direction is averaged. The resulting distributions of change of water content versus y-coord along the ligament of the beam are shown in Figure 14.

The inclusions have a strong influence on the shape of the water content curves. The larger the volume fraction, the lower is the water content inside the beam. For the present 2D idealisation, the consideration of inclusions results in a strong fluctuations in the water content curve, which has not been reported in the experiments. It is expected that a 3D model would predict a smoother curve if the average of water contents in the out of plane direction would be considered. Alternatively, the response of multiple 2D meso-scale analyses could be averaged.

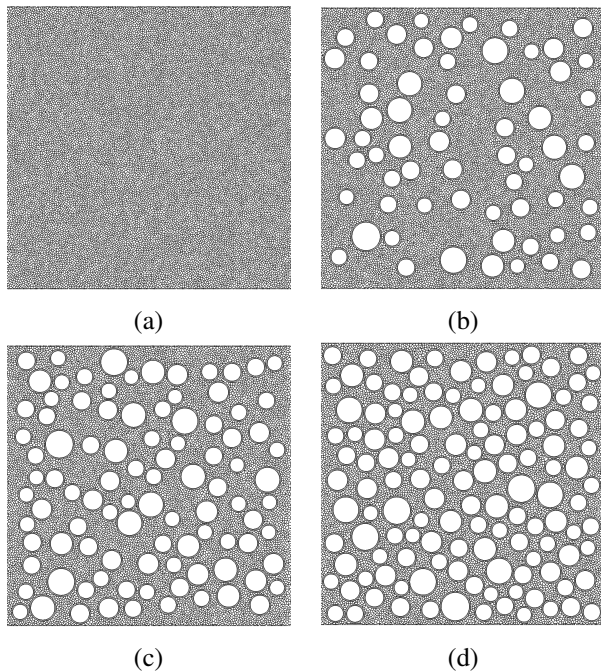


Figure 13: Meshes for the meso-scale transport analysis for aggregate volume fractions of (a)  $\rho = 0$ , (b) 0.2, (c) 0.3 and (d) 0.4.

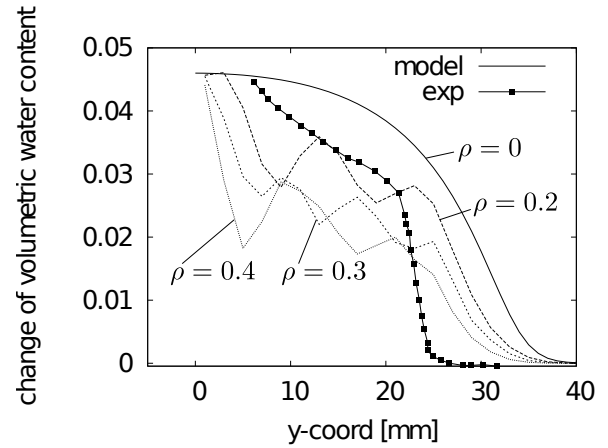


Figure 14: Change of water content versus y-coord along the ligament of the beam for aggregate volume fractions of  $\rho = 0, 0.2, 0.3$  and  $0.4$  at a time of 8 h compared to experimental results reported in [8].

## 5 Conclusions

In the present work, a dual lattice model for the coupling of fracture and water transport has been presented. The main conclusions can be summarised as follows:

The transport part of the coupled model based on homogeneous material properties represents well the transport of water through unsaturated porous concrete for the first few hours after the start of the absorption process. However, at later stages the water absorption is overestimated.

The model can simulate transport both within cracks and from cracks into the surrounding material by means of a single lattice.

By consideration of the meso-structure of concrete in the form of impermeable inclusions, the water absorption at later stages is in better agreement with experimental results than for the case of homogeneous properties.

## Acknowledgements

The simulations were performed with the object-oriented finite element package OOFEM [12, 13] extended by the present author.

## REFERENCES

- [1] Grassl, P., 2009. A lattice approach to model flow in cracked concrete. *Cement*

- and Concrete Composites*, **31**: 454–460.
- [2] Grassl, P. and Jirásek, M., 2010. Mesoscale approach to modelling the fracture process zone of concrete subjected to uniaxial tension. *International Journal of Solids and Structures*, **47**: 957–968.
- [3] van Genuchten, M. Th., 1980. A closed-form equation for predicting the hydraulic conductivity of unsaturated soils. *Soil Science Society of America*, **44**: 892–898.
- [4] Mualem, Y., 1976. A new model for predicting the hydraulic conductivity of unsaturated porous media. *Water Resources Research*, **12**: 513–522.
- [5] Vogel T., Van Genuchten M. Th. and Cislerova M., 2000. Effect of the shape of the soil hydraulic functions near saturation on variably-saturated flow predictions. *Advances in Water Resources*, **24**: 133–144, 2000.
- [6] Witherspoon P. A., Wang J. S. Y., Iawai K. and Galw J. E., 1980. Validity of cubic law for fluid flow in a deformable rock fracture. *Water Resources Research*, **6**:1016–1024, 1980.
- [7] Bolander, J. E. and Berton S., 2004. Simulation of shrinkage induced cracking in cement composite overlays. *Cement and Concrete Composites*, **26**: 861–871.
- [8] Wittmann, F. H., Zhang, P., Zhao, T., Lehmann, E. and Vontobel, P., 2008. Neutron radiography, a powerful method for investigating water penetration into concrete. In *Advances in Civil Engineering Materials, Proceedings of the 50-year teaching and research anniversary of Prof. Sun Wei*.
- [9] Baroghel-Bouny, V. and Mainguy, M. and Lassabatere, T. and Coussy, O., 1999. Characterization and identification of equilibrium and transfer moisture properties for ordinary and high-performance cementitious materials. *Cement and Concrete Research*, **29**: 1225–1238.
- [10] Meschke G. and Grasberger S., 2003. Numerical modelling of coupled hygromechanical degradation of cementitious materials. *Journal of Engineering Mechanics*, **129**: 383–392.
- [11] Wang L. and Ueda T., 2011. Mesoscale modelling of water penetration into concrete by capillary absorption. *Ocean Engineering*, **38**:519–528, 2011.
- [12] Patzák, B., 1999. Object oriented finite element modeling. *Acta Polytechnica*, **39**: 99–113.
- [13] Patzák B. and Bittnar Z., 2001. Design of object oriented finite element code. *Advances in Engineering Software*, **32**: 759–767.